EMAC 2003 Proceedings, eds. R.L. May & W.F. Blyth, Sydney 2003

Scaling and correlation analysis of the spiral galaxy M 51

A. Fletcher,[1] *J.I. Harnett,*[1,2] *P. Frick,*[3] *R. Beck,*[1] *E.M. Berkhuijsen*[1] *and I. Patrickeyev*[3]

[1] Max-Planck-Institut für Radioastronomie, Auf dem Hügel 69, D-53121 Bonn, Germany
E-mail: fletcher@mpifr-bonn.mpg.de
[2] University of Technology Sydney, PO Box 123, Broadway 2007, NSW, Australia
[3] Institute of Continuous Media Mechanics, Korolyov str. 1, 614061 Perm, Russia

1 Introduction

Recent improvements in astronomical hardware, such as adaptive optics, the advent of the Hubble Space Telescope, and an array of new ground and space-based instruments have resulted in superior resolution of optical, radio, infrared and X-ray telescopes in recent years. Consequently, the details visible in astronomical objects in many wavelength ranges have improved significantly. In nearby external galaxies, for example, not only is it now possible to resolve structures in bars and central regions, but also to detect individual star-forming regions in radio, X-ray and IR continuum and the spectral lines of ionised (H II), atomic (H I) and molecular (CO) gas components. An important question which can now be posed is: how are these different components of a galaxy related?

The choice of mathematical tool is of great importance for the scaling analysis of images and morevoer is often dependent on the quality and morphology of the data to be analysed. The structure function, for example, cannot resolve scales which are close to dominating large-scale structures. This in turn can lead to the erroneous interpretation that a continuous range of scales with a power law exists. Traditional Fourier techniques, applied to real data, give very spiky spectra, in which the separation of real maxima and high harmonics can be difficult.

Analysis is now possible, however, via the detection of similar structures in widely separated energy ranges and *wavelet spectrum* techniques. For data of sufficient quality, this new mathematical tool allows us to detect structures of different scales in data sets. First applications to astronomical objects showed that wavelets are effective in time series analysis [7, 8, 9] denoising [20, 4], structure detection [10] and image analysis [11].

The similarity of the far-infrared and radio continuum morphologies (e.g. in the nearby spiral galaxy M 31) indicates that magnetic fields are not anchored in the warm medium, but in cool gas clouds [15, 13]. On the other hand, CO line emission is correlated with radio continuum emission in spiral arms of M 31, but it is anticorrelated with the polarised radio emission [3].

Anticorrelations are often even more interesting than correlations and certainly more puzzling. In the spiral galaxy NGC 6946 a striking anticorrelation between the optical spiral arms and the "magnetic arms" seen in radio polarisation was discovered by Beck & Hoernes [1]. Although obvious to the eye, the analysis of this phenomenon needs sophisticated techniques. Based on wavelet analysis, Frick et al. [10] showed that the "magnetic arms" are phase-shifted images of the optical arms. Dynamo models are able to generate such structures [17].

The existence of a correlation, anticorrelation or non-correlation also has important consequences for the interpretation of observable quantities which emerge from a combination of physical quantities. For example, Faraday rotation (RM) of polarised radio waves is due to the product of electron density ($n_{\rm e}$) and the magnetic field component along the line of sight ($B_{||}$), integrated along the line of sight. Knowledge of $< n_{\rm e} >$, where $< \ldots >$ denotes an average value along the line of sight, (e.g. from observations of pulsars) is not sufficient to determine the strength of $< B_{||} >$ unless it is known whether $n_{\rm e}$ and $B_{||}$ are correlated, anticorrelated or non-correlated [2].

In the next two sections we briefly describe the use of wavelets in scaling and correlation analysis. For a deeper discussion of the method see Frick et al. [11].

2 Wavelets as a tool for scaling analysis

Wavelet analysis is based on a space-scale decomposition using the convolution of the data with a family of self-similar basis functions that depend on two parameters, scale and location. It can be considered as a generalization of the Fourier transformation, which uses harmonic functions as a one-parameter functional basis, characterized by frequency, or in the case of a space function, by the wavevector $\vec{k}$. The wavelet transformation also uses oscillatory functions, but in contrast to the Fourier transform these functions rapidly decay towards infinity. The family of functions is generated by dilations and translations of the mother function, called the analysing wavelet. This procedure provides self-similarity, which distinguishes the wavelet technique from the windowed Fourier transformation, where the frequency, the width of the window and its position are independent parameters.

We consider the continuous wavelet transform, which in the two-dimensional case can be written in

the form

$$W(a,\vec{x}) = \frac{1}{a^\kappa}\int_{-\infty}^{+\infty}\int_{-\infty}^{+\infty} f(\vec{x}')\psi^*\left(\frac{\vec{x}'-\vec{x}}{a}\right)d\vec{x}'. \quad (1)$$

Here $\vec{x} = (x,y)$, $f(\vec{x})$ is a two-dimensional function, for which the Fourier transform exists, $\psi(\vec{x})$ is the analysing wavelet (real or complex, with * denoting the complex conjugation), a is the scale parameter, and κ is a normalization parameter which will be discussed below. The wavelet must have a mean value of zero and so, by the convolultion theorem, the mean value of $W(a,\vec{x})$ is also zero.

The relation between an isotropic wavelet and the Fourier transform is defined as follows: the Fourier transform $\hat{f}(\vec{k})$ of the function $f(\vec{x})$ is given as

$$\hat{f}(\vec{k}) = \int_{-\infty}^{+\infty}\int_{-\infty}^{+\infty} f(\vec{x})e^{-i\vec{k}\cdot\vec{x}}d\vec{x},$$

where $\vec{k} = (k_x, k_y)$ is the wavevector. Then the inverse Fourier transform is

$$f(\vec{x}) = \frac{1}{4\pi^2}\int_{-\infty}^{+\infty}\int_{-\infty}^{+\infty} \hat{f}(\vec{k})e^{i\vec{k}\cdot\vec{x}}d\vec{k}$$

and the wavelet coefficients (Equation 1) can be expressed as

$$W(a,\vec{x}) = \frac{a^{2-\kappa}}{4\pi^2}\int_{-\infty}^{+\infty}\int_{-\infty}^{+\infty} \hat{f}(\vec{k})\hat{\psi}^*(a\vec{k})e^{i\vec{k}\cdot\vec{x}}d\vec{k}.$$

We restrict our analysis to the use of *isotropic* wavelets, which means that the analysing wavelet is an axisymmetric function $\psi = \psi(\rho)$, $\rho = \sqrt{x^2+y^2}$. The choice of the wavelet function depends on the data and on the goals of the analysis. For local structure recognition a function well localized in the physical space, is preferable.

For analysis of M 51 our choice of the wavelet was determined by the wish to have more independent points for further structure analysis which led to a simple real isotropic wavelet with a minimal number of oscillations, known as the *Mexican Hat*

$$\psi(\rho) = (2-\rho^2)e^{-\rho^2/2}. \quad (2)$$

We shall refer to this function as MH; it is shown in Figure 1.

The wavelet transform (1) is unique and reversible which means that the analysed function $f(x,y)$ can be reconstructed from its wavelet decomposition. In our analysis we do not need the inverse transform and do not give the reconstruction formula. (An extended description of continuum wavelet transform can be found in [14] and [21].)

3 Wavelet spectra and cross-correlations

To illustrate how wavelets decompose the image in different scales we show in Figure 2, the total radio emission image,at a wavelength of 6 cm, of the galaxy

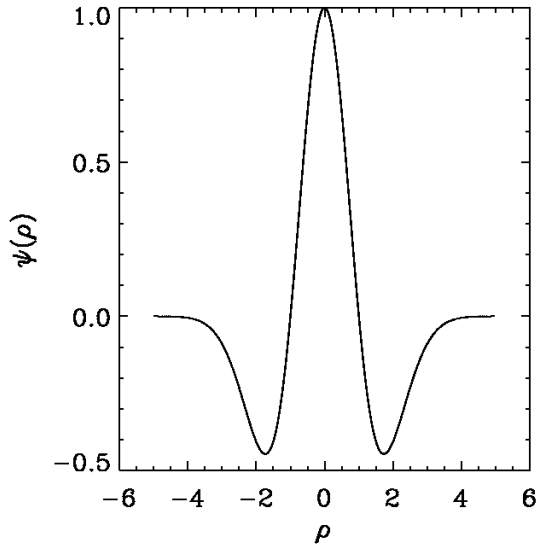

FIGURE 1. The isotropic MH wavelet function used in this paper.

M 51 and its wavelet coefficients $W(a,\vec{x})$ for three different scales a.

The distribution of energy among different scales is characterized by the wavelet spectrum, defined as the energy of the wavelet coefficients in a given scale a

$$M(a) = \int_{-\infty}^{+\infty}\int_{-\infty}^{+\infty} |W(a,\vec{x}|^2\, d\vec{x}. \quad (3)$$

We now discuss cross-correlations between different images of the same astronomical object. Consider two images (maps), $f_1(x,y)$ and $f_2(x,y)$, with the same angular resolution and the same number of pixels. The simplest way to conduct a linear correlation study is by the direct calculation of the "standard" correlation coefficient pixel by pixel:

$$r_p = \frac{\sum(f_{1i} - < f_1 >)(f_{2i} - < f_2 >)}{(\sum(f_{1i} - < f_1 >)^2 \sum(f_{2i} - < f_2 >)^2)^{1/2}}, \quad (4)$$

where i is number of a pixel. The accuracy of this estimate depends on the degree of correlation and on the number of *independent* points n in the map (see, for example, [5])

$$\Delta r = \frac{\sqrt{1-r^2}}{\sqrt{n-2}}\,. \quad (5)$$

This correlation coefficient is a global value which contains all the scales present in the images, including the largest one. The latter shows that the maxima of the extended intensity distributions coincide in position at most wavelengths. However, we wish to know whether the correlation coefficient depends on scale so we introduce the correlation coefficient for a given scale a:

$$r_w(a) = \frac{\int\int W_1(a,\vec{x})W_2^*(a,\vec{x})d\vec{x}}{(M_1(a)M_2(a))^{1/2}}\,. \quad (6)$$

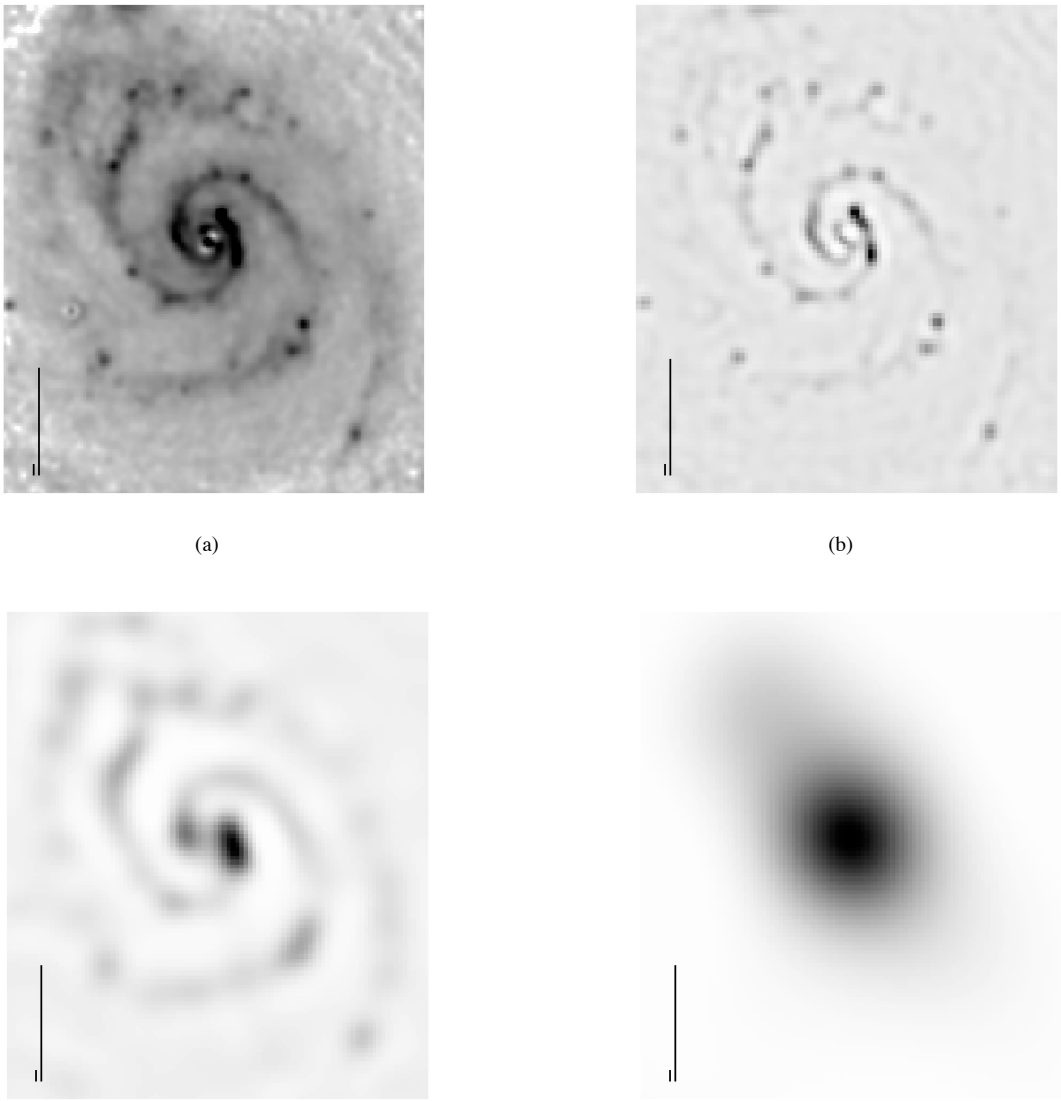

FIGURE 2. Images of the 6 cm total radio emission (central peak subtracted) and its wavelet decompositions for 3 different scales: $10''$, $50''$ and $100''$. Top row (from left to right): (**a**) original map, (**b**) map of the wavelet coefficients for the scale $10''$ Bottom row: (**c**) same as (b) but for the scale $50''$, (**d**) same as (b) but for the scale $100''$. The size of every image is $6'34'' \times 7'36''$. The two vertical lines are $10''$ and $100''$ long.

To estimate the error $\Delta r_w(a)$ we use Equation (5) taking $n = L_x L_y / a^2$, where $L_x L_y$ gives the area of the map in pixels.

4 The Data

M 51 is a grand design spiral galaxy with two major arms through which an intricate pattern of dust lanes weaves. Dust is also present in the inter-arm regions and can be seen emerging from the bright central bulge which envelopes the nucleus. The galaxy is probably interacting with a companion galaxy. Interactions usually imply enhanced localised star formation rates as shear forces compress the gas and dust. The two principle arms can be traced through more than $360°$ in azimuth and numerous ionised hydrogen (H II) regions are apparent. As well as discrete H II regions, there are large blobs or bubbles, rich in H II in the arms. A distance of 9.6 Mpc to the galaxy is assumed.

Data in many spectral ranges are available. For our analysis we used:

(a) The total radio continuum emission at the wavelength 6 cm (I6), obtained by combining observations with the NRAO Very Large Array (VLA) synthesis telescope and the 100m Effelsberg single dish telescope [6]. This emission is mainly synchrotron radiation, produced by relativistic *cosmic ray electrons* spiralling along interstellar *magnetic field* lines.

(b) The linearly polarised radio continuum emission at the wavelength 6 cm, again obtained from combined observations with the VLA and Effelsberg telescope [6]. The polarised radio emission traces the large scale, *regular magnetic field*.

(c) The Hα line emission (Balmer α line) of ionised hydrogen integrated over the whole frequency width of the line [12]. Hα emission comes from hydrogen that has been ionised by ultraviolet radiation from young, massive stars. *The ionised gas* is therefore a tracer of recent massive star formation. The temperatures of this gas is 7000–10000 K.

(d) The radio line emission of neutral atomic hydrogen H I at λ21.1 cm (H I) observed with the VLA, integrated over the whole frequency width of the line [18]. H I is overwhelmingly the most abundant form of neutral *atomic gas* in the interstellar medium.

(e) The (1-0) line emission of the carbon monoxide molecule (CO) at the wavelength 2.6 mm observed with the BIMA interferometer, integrated over the whole frequency width of the line [16]. The CO emission is the best available tracer of the *molecular gas* in galaxies. This gas is predominately H_2, but this molecule is difficult to observe directly.

(f) The mid-infrared emission (wavelength 12–18 μm) observed with the ISOCAM camera on board the ISO satellite [19]. This wavelength range is dominated by the band of emission lines from polycyclic aromatic hydrocarbons (PAHs) at 12.7 μm, but also includes continuum emission from small, warm dust grains. The strongest *dust* emission is a tracer of shocked regions which have been compressed by the passage of an underlying spiral density wave pattern. It is also distributed tenuously, but evenly throughout the galaxy.

All maps were transformed to the same resolution ($8''$, corresponding to 370 pc at the assumed distance to the galaxy), area ($6'34'' \times 7'36''$) and pixel size ($2''$). Each map contains 197×228 pixels.

5 Spectral Characteristics

The wavelet spectra of the six maps are shown in Figure 3.

We can infer and objectively quantify some key properties of the galaxy from the spectra. The magnetic field & cosmic rays, regular magnetic field and the dust emission all have spectral maxima at the largest scale. This is due to strong emission from the central regions of the galaxy (see Figure 2(d)).

The absence of a maximum in the spectrum of the magnetic field and cosmic rays, at the scale of the width of the clearly visible spiral arms $\simeq 20''$ is interesting. This means that the cross sectional profile of the spiral arms for this component of the interstellar medium (ISM) is far from being Gaussian (the approximate profile of the Mexican Hat wavelet); subsequent detailed examination of the data reveals that the emission profiles in cuts through the arms are strongly asymmetric and/or multi-peaked, with the emission increasing sharply at the inner edge of the arm (possibly as a result of shock compression) and then gradually decreasing. In contrast, the strong maximum in the molecular gas spectrum at $\simeq 30''$ not only quantifies the characteristic width of the strong molecular spiral arms, but also means that their profile is well fitted by the Mexican Hat wavelet with this scale. Closer examination of the emission profile shows that the molecular spiral arms are indeed roughly Gaussian in cross section, in contrast to the magnetic field and cosmic rays.

The regular magnetic field spectrum has a broad maximum at $\simeq 40''$, reflecting the extended arms of the regular magnetic field. The atomic gas and the ionised gas have similar spectra at small scales, due to the patches of strong emission from hydrogen clouds and star forming regions, respectively. The minimum in the ionised gas spectrum at $\simeq 150''$ shows the scale of the inter-arm regions, where star formation (the source of ionising UV photons) is much weaker than in the spiral arms. The maximum in the dust spectrum at $\simeq 90''$ is due to a strong emission disc in the centre of the map.

6 Cross Correlations

The wavelet cross correlations for six out of the 15 possible pairs of maps are shown in Figure 4. The top three panels show the correlation, scale by scale, of the magnetic field and cosmic rays with different tracers of the interstellar medium.

At the largest scales all of the images are well cor-

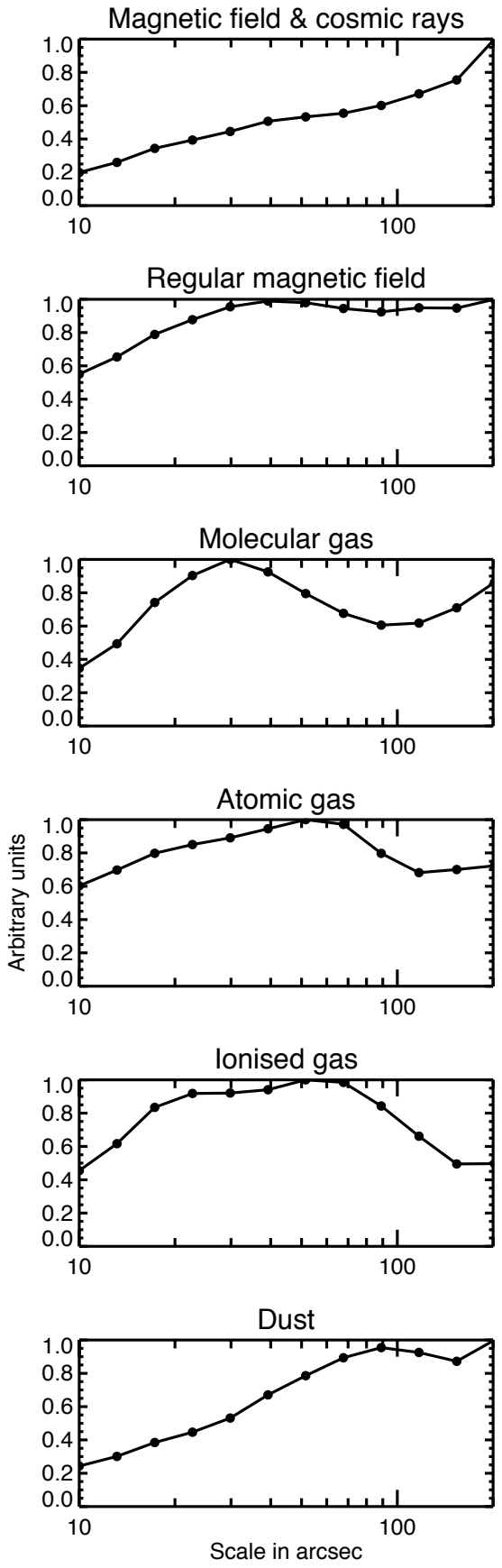

FIGURE 3. The spectral characteristics for different images of M 51.

related. However, at scales $\lesssim 50''$ we see that the correlation gets better as the gas becomes cooler and denser (dust is concentrated in the densest gas clouds). This somewhat counter-intuitive sequence can be qualitatively understood if we assume that the magnetic field is "frozen in" the interstellar medium (in other words a very high magnetic Reynolds number allows the plasma to be described by the equations of ideal magneto-hydrodynamics). Then we expect to find strong magnetic fields in the regions of highest gas density.

In the bottom three panels of Figure 4 we investigate how the ionised gas, heated by UV photons from massive young stars, is correlated with other parts of the ISM. The low correlation between atomic and ionised gas on small scales shows that when the UV field is strong enough to ionise hydrogen, it tends to be strong enough to ionise most of the atomic gas on scales of a few hundred parsec. The minimum in the correlation at a scale $\simeq 150''$ is due to the absence of atomic hydrogen emission in the centre of the galaxy; this is typical in spiral galaxies where most of the gas in the central regions is molecular hydrogen. At small scales the molecular and ionised gas phases are uncorrelated, due to the strong, well defined arms consisting of molecular gas. At all scales, the ionised gas is best correlated with the dust emission. This is to be expected as the heating source for both phases is thought to be recently formed massive stars. The slightly weaker correlation at the smallest scales can be interpreted as a sign of dust destruction in the region closest to the star forming regions; the complex PAH molecules are expected to disintegrate in hard UV fields.

7 Conclusions

The wavelet transform is a powerful technique for identifying structure in astronomical images and for making comparisons between different images. Scale separation of an image gives an objective measure of the characteristic size of dominant features, such as the width of spiral arms of molecular gas, and can also be used to infer other properties, such as the non-Gaussian cross sectional profiles of the spiral pattern of magnetic fields and cosmic rays, discussed in Section 5. The wavelet cross-correlation function allows a quantitative comparison of different images to be made on a scale by scale basis and hence leads to a deeper understanding of the data than the standard correlation coefficient. In Section 6 we showed that different images can be well correlated at some scales but poorly correlated at others; in trying to understand these differences we gain insight into the physical processes at work in the interstellar medium.

Acknowledgments

We thank Anvar Shukurov for useful discussions and the referees for helpful comments.

This research has made use of the NASA/IPAC

Extragalactic Database (NED) which is operated by the Jet Propulsion Laboratory, California Institute of Technology, under contract with the National Aeronautics and Space Administration.

JIH is grateful to the Max-Planck-Institut für Radioastronomie for support and hospitality.

The National Radio Astronomy Observatory is a facility of the National Science Foundation operated under cooperative agreement by Associated Universities, Inc.

References

[1] Beck, R. and Hoernes, P., Magnetic spiral arms in the galaxy NGC 6946, *Nature*, **379**, 1996, 47–49.

[2] Beck, R., Shukurov, A., Sokoloff, D. and Wielebinski, R., *Astron. Astrophys.*, submitted, 2003.

[3] Berkhuijsen, E.M., Bajaja, E. and Beck, R., CO observations of a region of strongly polarized radio continuum emission in the SW arms of M31, *Astron. Astrophys.*, **279**, 1993, 359–375.

[4] Chen, P.C., Zhang, X.Z., Xiang, S.P., Feng, L.L. and Reich, W., Application of Debauchies wavelet to the de-noising of radio maps, *Chin. Astron. Astrophys.*, **25**, 2000, 132–137.

[5] Edwards, A.L., *Multiple Regression and Analysis of Variance and Covariance,* W.H. Freeman and Company, San Francisco, 1979.

[6] Fletcher, A., Beck, R., Berkhuijsen, E.M., Horellou, C. and Shukurov, A., in preparation, 2003.

[7] Foster, G., Wavelets for period analysis of unevenly sampled time series, *Astron. J.*, **112**, 1996, 1709–1729.

[8] Frick, P., Baliunas, S.L., Galyagin, D., Sokoloff, D. and Soon, W., Wavelet Analysis of Stellar Chromospheric Activity Variations, *Astrophys. J.*, **483**, 1997, 426–434.

[9] Frick, P., Galyagin, D., Hoyt, D., Nesme-Ribes, E., Shatten, K., Sokoloff, D. and Zakharov, V., Wavelet analysis of solar activity recorded by sunspot groups, *Astron. Astrophys.*, **328**, 1997, 670–687.

[10] Frick, P., Beck, R., Shukurov, A., Sokoloff, D., Ehle, M. and Kamphuis, J., Magnetic and optical spiral arms in the galaxy NGC 6946, *Mon. Not. R. Astron. Soc.*, **318**, 2000, 925–937.

[11] Frick, P., Beck, R., Berkhuijsen, E.M. and Patrickeyev, I., Scaling and correlation analysis of galactic images, *Mon. Not. R. Astron. Soc.*, **327**, 2001, 1145–1157.

[12] Greenawalt, B., Walterbos, R.A.M., Thilker, D. and Hoopes, C.G., Diffuse ionized gas in M51/NGC 5195 and M81, *Astrophys. J.*, **506**, 1998, 135–151.

[13] Hoernes, P., Berkhuijsen, E.M. and Xu, C., Radio-FIR correlations within M 31, *Astron. Astrophys.*, **334**, 1998, 57–70.

[14] Holschneider, M., *Wavelets: An Analysis Tool,* Oxford University Press, Oxford, 1995.

[15] Niklas, S. and Beck, R., A new approach to the radio-far infrared correlation for non-calorimeter galaxies, *Astron. Astrophys.*, **320**, 1997, 54–64.

[16] Regan, M.W., Thornley, M.D., Helfer, T.T., Sheth, K., Wong, T., Vogel, S.N., Blitz, L. and Bock, D.C.-J., The BIMA Survey of Nearby Galaxies. I. The Radial Distribution of CO Emission in Spiral Galaxies, *Astrophys. J.*, **561**, 2001, 218–237.

[17] Rohde, R., Beck, R. and Elstner, D., Magnetic arms in NGC 6946 generated by a turbulent dynamo,*Astron. Astrophys.*, **350**, 1999, 423–433.

[18] Rots, A.H., Bosma, A., van der Hulst, J.M., Athanassoula, E. and Crane, P.C., High resolution H I observations of the Whirlpool galaxy M51, *Astron. J.*, **100**, 1990, 387–393.

[19] Sauvage, M., Blommaert, J., Boulanger, F., et al., ISOCAM mapping of the Whirlpool galaxy M 51, *Astron. Astrophys.*, **315**, 1996, L89–92.

[20] Tenorio, L., Jaffe, A.H., Hanany, S. and Lineweaver, C.H., Applications of wavelets to the analysis of cosmic microwave background maps, *Mon. Not. R. Astron. Soc.*, **310**, 1999, 823–834.

[21] Torresani, B., *Continuous Wavelet Transform,* Savoire, Paris, 1995.

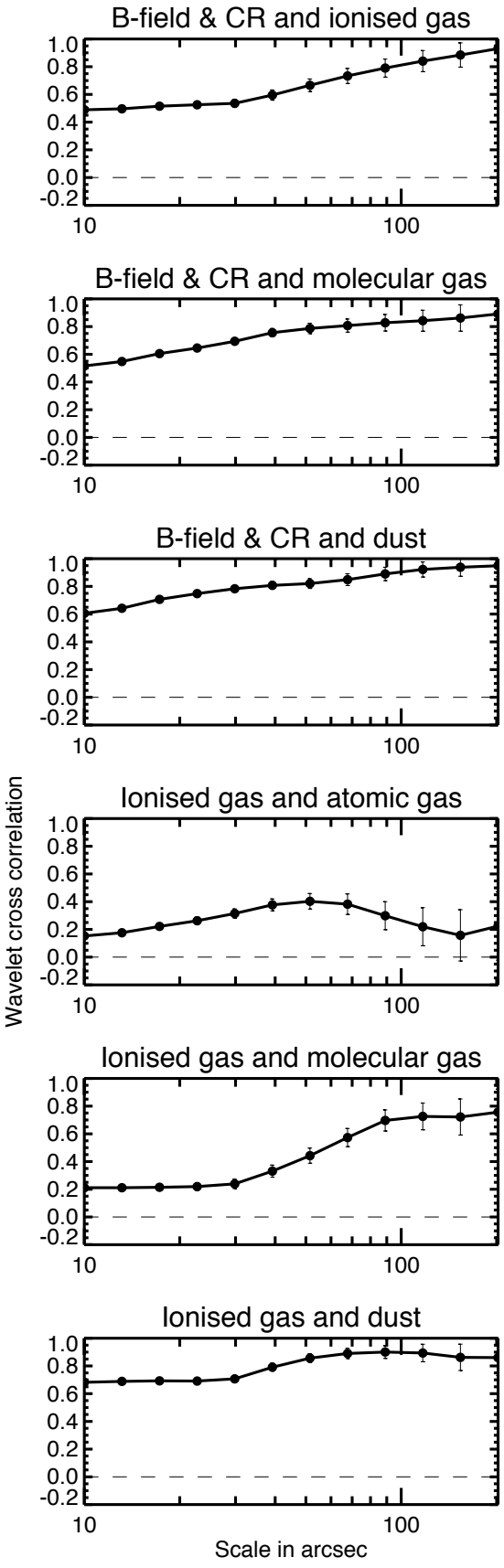

FIGURE 4. Wavelet cross correlation characteristics of M 51. In the top three panels the title 'B-field & CR' refers to the total magnetic field and cosmic rays.